Two-band superconductivity of lead probed by scanning tunneling spectroscopy

Michael Ruby[1], Benjamin W. Heinrich[1], Jose I. Pascual[1,2], Katharina J. Franke[1]
[1] *Fachbereich Physik, Freie Universität Berlin, Arnimallee 14, 14195 Berlin, Germany.*
[2] *CIC nanoGUNE and Ikerbasque, Basque Foundation for Science, Tolosa Hiribidea 78, Donostia-San Sebastian 20018, Spain*
(Dated: December 15, 2014)

The type I superconductor lead (Pb) has been theoretically predicted to be a two-band superconductor. We use scanning tunneling spectroscopy to resolve two superconducting gaps with an energy difference of 150 μeV. Tunneling into Pb(111), Pb(110) and Pb(100) crystals reveals a strong dependence of the two coherence peak intensities on the crystal orientation. We show that this is the result of a selective tunneling into the two bands at the energy of the two coherence peaks. This is further sustained by the observation of signatures of the Fermi sheets in differential conductance maps around subsurface defects. A modification of the density of states of the two bands by adatoms on the surface confirms the different orbital character of each of the two sub-bands.

PACS numbers: 73.20.-r 74.25.Jb, 74.55.+v

The theory of Bardeen, Cooper and Schrieffer (BCS) has been extremely successful in describing many aspects of superconductivity (SC). It predicts the formation of a condensate of quasi-particles, the so-called Cooper pairs, as a result of electron-phonon coupling. The corresponding quasi-particle excitation spectrum exhibits a characteristic gap of width 2Δ around the Fermi level, with Δ being the order parameter reflecting the bonding strength of the Cooper pairs. However, soon after the development of the BCS formalism, it was realized that the theory has to be extended for describing the properties of even the simplest elemental superconductors such as Pb, V, Ta, *etc.* In particular, two quasiparticle resonances have been observed in planar Pb tunneling junctions [1–4]. The initial interpretations of these experiments proposed an anisotropic electron-phonon coupling leading to a **k**-dependent order parameter as the origin of this behavior [5].

With the discovery of superconductivity in highly anisotropic, composite materials, such as MgB_2, $NbSe_2$, CaC_6, *etc.* with two distinct energy gaps and unexpectedly high critical temperatures [6–14], the importance of the concept of multi-band superconductivity, which had been proposed already in 1959 [15], was realized. This motivated a renewed theoretical treatment of conventional superconductors with state-of-the-art methods. These revealed that two disjoint Fermi sheets (FS) with different electron-phonon coupling strengths lead to two distinct energy gaps and an increased critical temperature as compared to a single isotropic gap [16].

Floris *et al.* identified by density functional theory (SCDFT) that two-band superconductivity also plays a role in the elemental superconductor Pb [17]. They found that the Fermi surface of Pb is composed of a compact Fermi sheet with mostly *s*-*p*-character and a tubular Fermi sheet of *p*-*d*-character. The different orbital nature leads to different electron-phonon coupling strengths [18], and causes different pairing energies in the SC condensate.

Experimentally, it is difficult to distinguish between a two-band model and an anisotropic variation of the order parameter. Angle-resolved photoemission spectroscopy, a prime candidate for experimental band structure determination, lacks the required energy resolution. Planar tunneling junctions have revealed two peaks in the gap structure [1–4], but the tunneling current is the sum of all tunneling paths including step edges, vacancies, impurities, etc. This prohibits an unambiguous interpretation of the tunneling spectra.

Here, we overcome this shortcoming using scanning tunneling microscopy and spectroscopy to probe atomically-flat surfaces as well as well-defined defects and distinguish between the different contributions to tunneling. We present direct evidences for the two-band nature of superconductivity in Pb. Two BCS-like resonances with an energy separation of 150 μeV are observed. Depending on the surface orientation the intensity of these peaks varies due to **k**-selective tunneling into the two Fermi sheets. Scattering patterns around sub-surface Ne impurities at the energies of the two coherence peaks reveal signatures of the shape of the respective Fermi sheets as a result of an anisotropic electron propagator in the crystal [19–22]. Furthermore, we show that the distinct orbital character of the Fermi sheets is reflected by the modification of density of states at adatoms, which tends to increase the weight of tunneling into more localized *d*-states over the delocalized *s*-*p*-derived states.

Our experiments were carried out in a Specs JT-STM under ultra-high vacuum conditions at a base temperature of 1.2 K. Pb is a type I superconductor with a critical temperature of $T_c = 7.2$ K and a coherence length of 83 nm. The single crystals were cleaned by cycles of Ne^+ ion sputtering at 900 eV with a Ne pressure of 1.5×10^{-4} mbar (background pressure: $< 1.5 \times 10^{-9}$ mbar) and annealing to 430 K for 30 min until a clean, atomically flat and superconducting surface was observed. To achieve high energy resolution we cover etched W-tips with Pb by deep indentations into the clean Pb surface

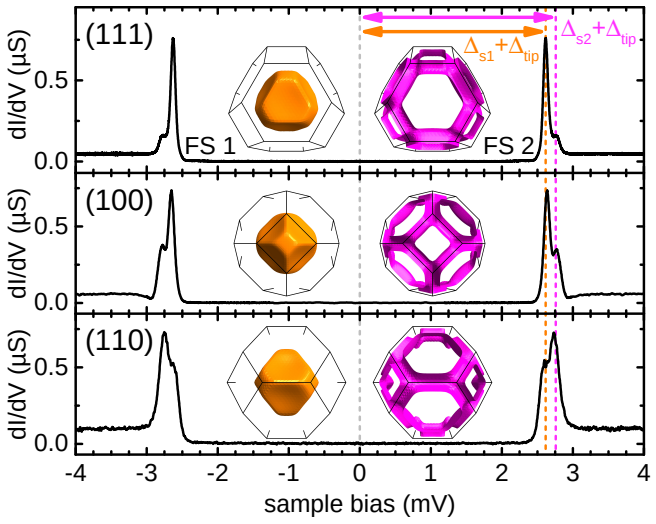

FIG. 1. $\mathrm{d}I/\mathrm{d}V(V)$-spectra on clean terraces of Pb(111), (100), and (110) single crystal surfaces. The superconducting gap around E_F is framed by QPRs at $\approx\pm2.7\,\mathrm{mV}$, consisting of two peaks separated by $\approx150\,\mu\mathrm{eV}$. The energy of the peaks is given as the sum of the pairing energy of the tip (Δ_tip) and the sample (Δ_{s1} and Δ_{s2}, respectively). The insets show the corresponding top views on the two FS sheets of a Pb single crystal. 3D-models from [25]. Lock-in modulation amplitude was $15\,\mu\mathrm{V_{rms}}$ at 912 Hz.

until superconductor-superconductor tunneling spectra are measured [23] (see Supplemental Material for details [24]). The use of a superconducting tip together with an elaborated grounding and RF-filtering scheme yields an effective energy resolution of $\approx45\,\mu\mathrm{eV}$ at 1.2 K (compared to $\approx$ 360 μeV with a normal metal tip, in which Fermi-Dirac broadening limits the energy resolution). Crystalline directions were determined by atomically resolved topographies of the clean Pb surface (see Fig. S1 [24]).

We record $\mathrm{d}I/\mathrm{d}V(V)$ spectra on clean terraces of the three low-index surfaces (111), (100), and (110) of Pb single crystals to probe their superconducting energy gaps (Fig. 1). Around E_F, the superconducting gap (zero conductance) is framed by quasi-particle resonances (QPR) at $\approx\pm2.7\,\mathrm{meV}$ [26]. In the spectra of all surface orientations, we observe two pairs of QPRs separated by $\approx150\,\mu\mathrm{eV}$ [27]. Due to the superconducting state of the tip, the spectra are a convolution of two SC density of states. In particular the position of the QPRs is shifted by Δ_tip. To extract the exact energy positions and intensities of the two QPRs, we deconvolute the spectra as described in the Supplemental Material [24]. We can unambiguously link the appearance of the two peaks with $\approx150\,\mu\mathrm{eV}$ separation to a property of all samples, independent of the tip's single gap. Similar splittings have been observed earlier in planar Pb tunnel junctions and attributed to the anisotropic FS and electron-phonon coupling of Pb [1, 3–5]. More recently however, Floris *et al.* predicted that Pb is a two-band superconductor with two well-separated highly anisotropic Fermi sheets (see inset in Fig. 1) [17]. The inner FS (FS1) has an almost spherical shape. The outer FS (FS2) has a tubular shape [28]. FS1 is mostly of *s*-*p* character with a smaller pairing energy than FS2 which is of *p*-*d*-like character [17]. A manifestation of the different pairing energy associated to each FS is the different position of the corresponding quasi-particle resonances QPR1 and QPR2 in the $\mathrm{d}I/\mathrm{d}V(V)$ spectra. Hence, we identify the inner and outer peaks as tunneling into FS1 and FS2 of the sample, respectively. The existence of a single gap in the STM tip is in agreement with its expected micro-crystalline character [29]. While the energy separation between QPR1 and QPR2 is constant for all surfaces, we observe distinct relative peak intensities for the different surface orientations (Fig. 1). The tunneling probability depends on transition matrix elements, which depend on the $k_\perp$ component of the wavevector $\boldsymbol{k}$. A strong tunneling contribution thus requires access to the FS sheets with the wavevector $\boldsymbol{k}$ being mostly perpendicular to the surface. The insets in Fig. 1 show the top views of the two FS sheets for the given crystal orientations. FS1 is compact, which implies that tunneling with strong $k_\perp$ contribution into the (111)-, (100)- and (110)-surface is possible. In contrast to this, FS2 exhibits open pores along the $\boldsymbol{k}_{\Gamma\to L}$- and $\boldsymbol{k}_{\Gamma\to X}$-direction. Hence, for these directions tunneling into FS2 is only possible with wavevectors with considerable $k_\parallel$ component, which is accompanied by a reduced tunneling probability. Therefore, the tunneling ratio FS1/FS2 is largest on the (111)-surface, where FS2 exhibits the largest pore, followed by the (100)-surface. On the (110)-surface, QPR2 is even more intense than QPR1 (see Supplemental Material for a quantitative analysis of the intensities [24]). Both FSs can be accessed by $\boldsymbol{k}$ vectors with mostly $k_\perp$ contribution and therefore participate almost equivalently in tunneling.

The observed energy splitting in STS together with the dependence of the QPR intensities on the surface orientation agrees well with the two-band superconductivity in the FSs of Pb as predicted by Floris *et al.* [17]. The difference between the pairing energies of $\approx10\,\%$ is however smaller than calculated ($\approx30\,\%$ [17]). We link this to interband scattering, which diminishes the difference in the pairing energy of the two bands [30].

We now search for a more direct evidence of the presence of the two FSs with different order parameter. One way to image the different symmetries of the two FSs is to inspect $\mathrm{d}I/\mathrm{d}V$ maps around buried impurities which show characteristic modulations of the DoS around them (Fig. 2 and Fig. S3 in the Supplemental Material [24]). On the Pb(100) surface we find typical patterns in STM topographies (see Fig. S2 [24]). These consist of a bright or dark center, which is framed by patterns of fourfold symmetry.

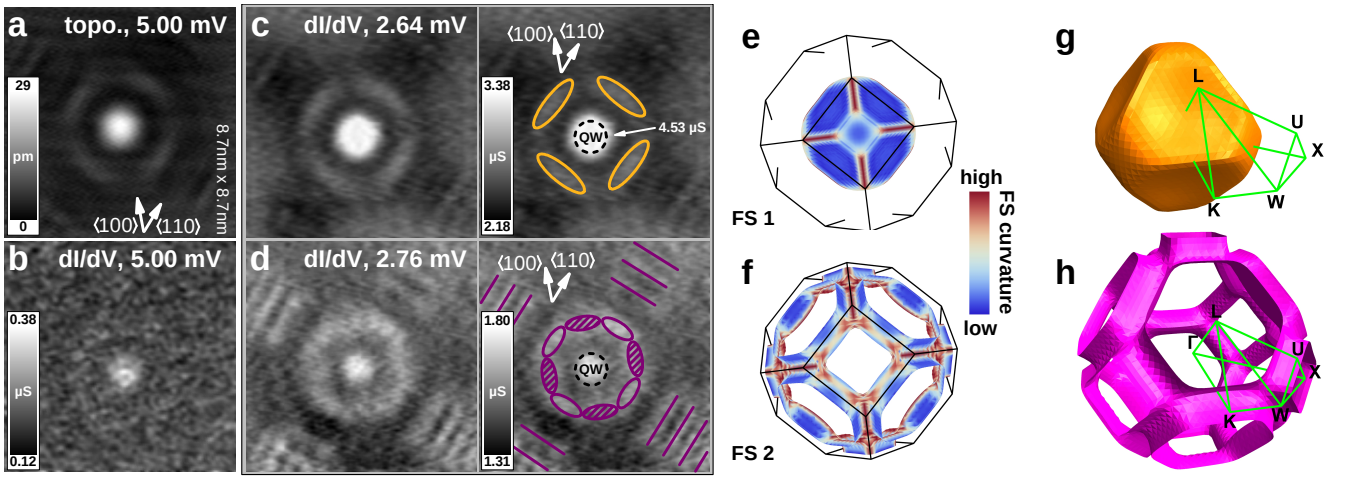

FIG. 2. (a–d) Subsurface Ne inclusion. High-resolution topography (a) on an atomically flat Pb(100) terrace (setpoint: 5 mV, 250 pA). Constant-height $\mathrm{d}I/\mathrm{d}V$ maps at 5 mV (b), 2.64 mV (c), and 2.76 mV (d) (25 $\mu\mathrm{V}_{\mathrm{rms}}$, 912 Hz, setpoint: 5 mV, 500 pA). In the duplicated maps, prominent scattering signatures are highlighted as guide for the eye. A quantum well state between the impurity and the surface leads to the higher conductance in the center of all maps. Note that the topography in (a) combines features visible in (c) and (d) because at a sample bias of 5 mV all states between E_{F} and $E_{\mathrm{F}}+5$ mV, *i.e.*, both Fermi sheets, contribute to the tunneling current. (e–h) 3D-models of the two FSs of Pb from Ref. [25]. The curvature of the FS is color-coded onto the 3D model in (e) and (f), which are oriented according to the crystalline directions in (a–d). *Dark blue* and *dark red* correspond to low and high curvature, respectively. Black lines in (e) and (f) mark the boundaries of the first Brillouin zone.

The impurities are most likely Ne-filled subsurface nanocavities, which are residuals of the Ne^+ ion sputtering [20, 31]. They act as scattering centers and give rise to quantum well states between the surface and the impurity [31]. The subsurface inclusion appears then as a protrusion or a depression, depending on whether or not the sample bias matches the quantization condition of the quantum well state. The quantum-well state typically has a width of several hundreds of meV (*e.g.* Fig. S3h in the Supplemental Material). Therefore it is present in a wide energy range. Laterally away from the impurity center the two constant-height $\mathrm{d}I/\mathrm{d}V$ maps at the energy of the two QPRs show quite different patterns of charge density oscillations. The map at 2.64 meV, which results from tunneling into QPR1, exhibits a square-like pattern with the edges along the ⟨110⟩ directions around the bright center (highlighted by *orange ellipses* in Fig. 2c). The map at the energy of QPR2 (2.76 meV, Fig. 2d) shows areas of high intensity along the ⟨100⟩ (*shaded purple ellipses*) and ⟨110⟩ (*open purple ellipses*) directions, respectively. Additionally, long-ranging oscillations appear in the $\mathrm{d}I/\mathrm{d}V$ signal along the ⟨110⟩ directions (indicated by *purple stripes*).

According to Weismann and co-workers, the charge density oscillations result from scattering and focusing of bulk electrons (holes) at subsurface impurities with an anisotropic electron (hole) propagation [21]. In analogy to Huygens principle, the group velocity of the electrons (holes) $\mathrm{d}E/\mathrm{d}k$ is perpendicular to the FS and therefore nearly parallel for beams arising from areas of low FS curvature. This leads to a focusing of the electron propagator into the normal direction of these regions [19]. Hence, the real space distribution of the DoS on the surface above the impurity, which is resolved via $\mathrm{d}I/\mathrm{d}V$ mapping, is directly related to the shape of the FS.

We can now assign the features of the $\mathrm{d}I/\mathrm{d}V$ maps to low-curvature regions of FS1 and FS2, respectively. The curvature of the respective FSs is color-coded onto the 3D models in Fig. 2(e,f). FS1 contains two groups of low-curvature regions (*dark blue* in Fig. 2e): eight large regions with the group velocity (*i.e.* FS surface normal) pointing into the ⟨111⟩ directions, *i.e.*, along the Γ-*L*-direction, and six smaller regions with the surface normal pointing towards ⟨100⟩, *i.e.* along the Γ-*X*-direction. Projected on the (100) surface, we can assign the four square-like stripes of high conductance (*orange ovals in Fig. 2c)* to the focusing of electron propagation in the ⟨111⟩ directions. Also for the ⟨100⟩ direction a higher intensity is expected. However, this direction is dominated by the quantum well state as discussed above. Both signals are superimposed and thus not distinguishable.

FS2 can be described as a complex structure with tubes connecting the *U*- and *W*-points, and connecting *K*- and *W*-points, respectively. Despite having a large three-dimensional curvature (Fig. 2h), the tubes exhibit one dimensional low curvature regions (lines). Along the line the group velocity is therefore pointing in the same direction, giving rise to an enhanced scattering pattern, in analogy to a decreased decay of Friedel oscillations in two dimensions [22]. The fourfold symmetry of the *U*-

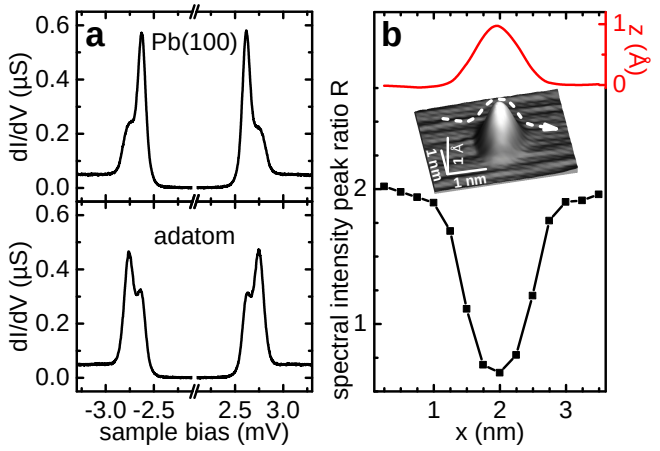

FIG. 3. Pb adatom on Pb(100). (a) $\mathrm{d}I/\mathrm{d}V(V)$ spectrum on clean Pb(100) (top) and on a Pb adatom (bottom). (b) Intensity ratio R of QPR1 vs. QPR2 and apparent height across a Pb adatom as sketched in the inset. R is determined by numerical deconvolution of the spectra as discussed in the Supplemental Material [24].

W- and K-W-tubes, respectively, then gives rise to the octagonal pattern (*purple ovals* in Fig. 2d) projected on the surface as seen in the $\mathrm{d}I/\mathrm{d}V$ map. The oscillations at larger distance can be linked to long-range interference of electrons (holes), due to scattering at side facets of the inclusion [20, 32] or due to interference of electrons (holes) with the same group velocity, but originating from different areas on the FS [22]. The distinct appearance of these patterns at QPR1 and QPR2 are thus a further proof of the geometrically very different FSs with different pairing energy.

According to the SCDFT calculations in Ref. [17] each FS has a different orbital character. We expect that this character will be reflected in the interaction with local potentials. Adsorbates interact with the electronic bands of the surface and locally modify the corresponding density of states. To probe this interaction with both the s-p-, and p-d-derived FSs, we deposited Pb adatoms from the lead-covered tip onto the surface by applying voltage pulses of 6 to 10 V at a tip–sample distance of approximately 1 nm. The inset of Fig. 3b shows a topography of an as-deposited adatom. The excitation spectrum above the center of the adatom (Fig. 3a, bottom) shows that QPR2 is more intense than QPR1, in contrast to the spectrum on the clean surface (Fig. 3a, top).

The spatial extension of this intensity variation is reflected in a series of spectra taken along a line over the adatom (see inset of Fig. 3b). The relative intensities $R = A_1/A_2$ of the QPRs, with A_1 and A_2 being the intensity of QPR1 and QPR2, respectively, after deconvolution are shown in Fig. 3b. The value decreases continuously from 2 over the clean surface to 0.65 on top of the adatom. Thus the adatoms increase the tunneling probability into FS2 compared to FS1. The variation of R is constricted to the adatom site [33]. In principle, a protruding feature such as an adatom geometrically favors tunneling with large $k_\perp$ contribution and may thus enhance the tunneling probability into FS1, leading to a larger R. The opposite trend observed in the experiment suggests another scenario. The increased intensity of QPR2 indicates that tunneling into the band of FS2 is particularly enhanced at the localized potential of the Pb adatom. This is a consequence of a strong confinement of localized d-derived states around an impurity potential. Therefore the band that is associated to FS2 and is hybridized with d-states is more affected than the extended s-p-bands that create FS1 [18].

Despite Pb being one of the best characterized type I superconductors, the theoretical prediction of Pb being a two-band superconductor was experimentally not unambiguously evidenced up to date. The early-on observed splitting of QPRs could either be described by an anisotropic electron-phonon coupling term or two distinct electronic bands at the Fermi level. We have shown clear fingerprints of the two-band nature of superconductivity in Pb. STS resolved the differing pairing energy on the two bands as 150 μeV, which is smaller than theoretically predicted. Calculations of interband scattering events may be able to explain this deviation. The energetically separated FSs allowed for a direct mapping of their symmetry in real space. This method is complementary to quasiparticle interference mapping by STM [34], which is frequently used to resolve characteristics of the FS of, *e.g.*, high-T_c superconductors. Most importantly, the intensity of quasiparticle interference falls off too rapidly in three-dimensional electron systems (such as Pb), and therefore requires two-dimensional states. Furthermore, it does not involve reconstruction of the Fermi surface by Fourier transformation, but directly reflects the symmetry of reciprocal space in real space.

The tuning of orbital contributions around atoms allows us in a proof-of-principle experiment to favor tunneling into one or the other FS and might be used – together with the focusing properties of the curved FSs – for **k**-selective filtering in future tunneling devices.

We gratefully acknowledge funding by the DFG through Sfb 658 and grant FR-2726/4.

[1] P. Townsend and J. Sutton, Phys. Rev. **128**, 591 (1962).
[2] G. I. Rochlin, Phys. Rev. **153**, 513 (1967).
[3] B. L. Blackford and R. H. March, Phys. Rev. **186**, 397 (1969).
[4] G. I. Lykken, A. L. Geiger, K. S. Dy, and E. N. Mitchell, Phys. Rev. B **4**, 1523 (1971).
[5] A. J. Bennett, Phys. Rev. **140**, A1902 (1965).
[6] F. Giubileo, D. Roditchev, W. Sacks, R. Lamy, D. X. Thanh, J. Klein, S. Miraglia, D. Fruchart, J. Marcus, and P. Monod, Phys. Rev. Lett. **87**, 177008 (2001).

[7] F. Giubileo, D. Roditchev, W. Sacks, R. Lamy, and J. Klein, Europhys. Lett. **58**, 764 (2002).

[8] C. Buzea and T. Yamashita, Supercond. Sci. Technol. **14**, R115 (2001).

[9] T. E. Weller, M. Ellerby, S. S. Saxena, R. P. Smith, and N. T. Skipper, Nature Physics **1**, 39 (2005).

[10] N. Bergeal, V. Dubost, Y. Noat, W. Sacks, D. Roditchev, N. Emery, C. Hérold, J.-F. Marêché, P. Lagrange, and G. Loupias, Phys. Rev. Lett. **97**, 077003 (2006).

[11] M. Calandra and F. Mauri, Phys. Rev. Lett. **95**, 237002 (2005).

[12] D. Roditchev, F. Giubileo, F. Bobba, R. Lamy, E.-M. Choi, H.-J. Kim, W. Kang, S. Miraglia, J. Marcus, W. Sacks, J. Klein, A. Cucolo, S.-I. Lee, and D. Fruchart, Physica C: Superconductivity **408410**, 768 (2004).

[13] N. Emery, C. Hérold, M. d'Astuto, V. Garcia, C. Bellin, J. F. Marêché, P. Lagrange, and G. Loupias, Phys. Rev. Lett. **95**, 087003 (2005).

[14] P. Martinez-Samper, J. Rodrigo, G. Rubio-Bollinger, H. Suderow, S. Vieira, S. Lee, and S. Tajima, Physica C: Superconductivity **385**, 233 (2003).

[15] H. Suhl, B. T. Matthias, and L. R. Walker, Phys. Rev. Lett. **3**, 552 (1959).

[16] H. J. Choi, D. Roundy, H. Sun, M. L. Cohen, and S. G. Louie, Nature **418**, 758 (2002).

[17] A. Floris, A. Sanna, S. Massidda, and E. K. U. Gross, Phys. Rev. B **75**, 054508 (2007).

[18] I. Y. Sklyadneva, R. Heid, P. M. Echenique, K.-B. Bohnen, and E. V. Chulkov, Phys. Rev. B **85**, 155115 (2012).

[19] J. Heil, M. Primke, K. U. Würz, and P. Wyder, Phys. Rev. Lett. **74**, 146 (1995).

[20] O. Kurnosikov, J. H. Nietsch, M. Sicot, H. J. M. Swagten, and B. Koopmans, Phys. Rev. Lett. **102**, 066101 (2009).

[21] A. Weismann, M. Wenderoth, S. Lounis, P. Zahn, N. Quaas, R. G. Ulbrich, P. H. Dederichs, and S. Blügel, Science **323**, 1190 (2009).

[22] S. Lounis, P. Zahn, A. Weismann, M. Wenderoth, R. G. Ulbrich, I. Mertig, P. H. Dederichs, and S. Blügel, Phys. Rev. B **83**, 035427 (2011).

[23] K. J. Franke, G. Schulze, and J. I. Pascual, Science **332**, 940 (2011).

[24] Supplemental Material available online.

[25] T.-S. Choy, J. Naset, S. Hershfield, C. Stanton, and J. Chen, in APS Meeting Abstracts (2000) p. 36042.

[26] Direct tunneling of Cooper pairs giving rise to a *dc* Josephson-current is not observed due to the weak overlap of the condensate wave functions at the experimental tip–sample distance.

[27] In the $\mathrm{d}I/\mathrm{d}V(V)$ spectrum on Pb(100) a dip is observed at $\pm 3\,\mathrm{mV}$. Such dips are occasionally resolved on all three surfaces and depend on the tip employed. They are due to deviations from pure BCS-like DoS originating from interband scattering [30].

[28] J. R. Anderson and A. V. Gold, Phys. Rev. **139**, A1459 (1965).

[29] P. Anderson, J. Phys. Chem. Solids **11**, 26 (1959).

[30] Y. Noat, T. Cren, F. Debontridder, D. Roditchev, W. Sacks, P. Toulemonde, and A. San Miguel, Phys. Rev. B **82**, 014531 (2010).

[31] M. Schmid, W. Hebenstreit, P. Varga, and S. Crampin, Phys. Rev. Lett. **76**, 2298 (1996).

[32] O. Kurnosikov, O. A. O. Adam, H. J. M. Swagten, W. J. M. de Jonge, and B. Koopmans, Phys. Rev. B **77**, 125429 (2008).

[33] Atomic modulation of the gap structure of multiband superconductors has been observed earlier [35]. Yet the modulation strength of the effect observed here is unexpectedly high and hints towards a strong modification of the LDoS at the adatom site.

[34] K. McElroy, R. W. Simmonds, J. E. Hoffman, D.-H. Lee, J. Orenstein, H. Eisaki, S. Uchida, and J. C. Davis, Nature **422**, 592 (2003).

[35] I. Guillamon, H. Suderow, F. Guinea, and S. Vieira, Phys. Rev. B **77**, 134505 (2008).